Geophysical Prospecting
EAGE EUROPEAN ASSOCIATION OF GEOSCIENTISTS & ENGINEERS

Geophysical Prospecting doi: 10.1111/j.1365-2478.2012.01053.x

Permeability inversion from low-frequency seismoelectric logs in fluid-saturated porous formations

Wei Guan*, Hengshan Hu and Zhi Wang

Department of Astronautics and Mechanics, Harbin Institute of Technology, Postbox 344, 92 West Dazhi Street, Harbin, 150001, China

Received November 2010, revision accepted August 2011

ABSTRACT

In this paper, a method is proposed to invert permeability from seismoelectric logs in fluid-saturated porous formations. From the analysis of both the amplitude and the phase of simulated seismoelectric logs, we find that the Stoneley wave amplitude of the ratio of the converted electric field to the pressure (REP) is sensitive to porosity rather than permeability while the tangent of the REP's phase is sensitive to permeability. The REP's phase reflects the phase discrepancy between the electric field and the pressure at the same location in the borehole. We theoretically derive the frequency-dependent expression of the REP of the low-frequency Stoneley wave and find that the tangent of the REP's argument is approximately in inverse proportion to permeability. We obtain an inversion formula and present the permeability inversion method by using the tangent of the REP's phase. To test this method, the permeabilities of different sandstones are inverted from the synthetic full-waveform data of seismoelectric logs. A modified inversion process is proposed based on the analysis of inversion errors, by which the relative errors are controlled below 25% and they are smaller than those of the permeability inversion from the Stoneley wave of acoustic logs.

Keywords: Borehole geophysics, Permeability, Inversion

INTRODUCTION

Permeability is one of the most important parameters for evaluating the level of difficulty in oil and gas exploitation. A quick, continuous and accurate insitu estimate of reservoir permeability is highly significant. In order to measure rock permeability by acoustic logs, the relation between permeability and borehole acoustic waves has been studied both theoretically and experimentally over the past several decades. Rosenbaum (1974) simulated acoustic logs in a porous formation by applying Biot's poroelastic wave theory (Biot 1956a,b; Biot 1962) and found the relationship between permeability and the borehole Stoneley wave. This model is therefore termed the Biot-Rosenbaum model. From acoustic logging data, Williams *et al*. (1984) also recognized that the velocity and the attenuation of the Stoneley wave are related to formation permeability. Winkler, Liu and Johnson (1989) performed laboratory experiments of measuring Stoneley wave propagation and found that the theoretical and experimental results agree well. Tang, Cheng and Toksöz (1991) developed a simplified Biot-Rosenbaum model to calculate the borehole Stoneley wave. Then Tang and Cheng (1996) proposed a fast inversion method to determine formation permeability from Stoneley wave logs. Wu *et al*. (1995) also inverted the permeability from the attenuation of the Stoneley wave. They compared the inverted permeabilities with both the values used in forward modelling and the measured permeabilities of rock cores.

However the relative errors in permeability inversion from Stoneley wave logs are too big in low-permeability formations, especially in high-porosity and low-permeability formations resulting from the high clay content in the pores. This is because the borehole Stoneley wave properties are influenced not only by permeability but also by formation elasticity, the

*E-mail: gwllzh@tom.com

content of clay in pores, mud cake on the borehole wall etc. (Cheng, Zhang and Daniel 1987). Thus more effective methods are expected to evaluate formation permeability. In recent years one potential method of using seismoelectric well logs has beenproposed (Zhu, Haartsen and Toksöz 1999; Singer *et al*. 2005).

The seismoelectric phenomenon was first found by Ivanov (1939), who recorded electric signals localized within a seismic wave propagating in the subsurface. Frenkel (1944) set up a theoretical framework to explain this phenomenon and concluded that it is due to an electrokinetic effect related to the relative fluid flow in porous media. The underground or subsea rock can be regarded as fluid-filled porous media composed of solid frames and pore fluid electrolytes. There is an electric double layer consisting of an absorbed layer and a diffuse layer near the surface of the solid grains (Morgan, Williams and Madden 1989). In the adsorbed layer, some kind of electrolyte ions (such as anions) is chemically adsorbed to the solid surface and the ions in this layer are assumed to be immovable. Surplus cations distributed in the diffuse layer are movable and balance the charge of the absorbed layer. When a seismic wave propagates in a porous medium, a relative movement between the fluid and the solid phase is generated, which carries the net charges in the diffuse layer and induces a convection electric current and an electromagnetic field. Conversely, an alternating electromagnetic field in the porous media which exerts forces on the net charges in the diffuse layer can produce the relative flow and a seismic field. These electrokinetic phenomena are respectively called seismoelectric and electroseismic conversions. Because of the relations with fluid conductivity, rock porosity, permeability, pore size, etc, people are interested in applying the electrokinetic coupling between seismic and electromagnetic fields to determine formation characteristics. With this background, borehole seismoelectric and electroseismic measurements are proposed and the signals are recorded in laboratory and field experiments (Zhu, Haartsen and Toksöz 1999; Mikhailov, Queen and Toksöz 2000; Hunt and Worthington 2000; Zhu and Toksöz 2003; 2005; Singer *et al*. 2005; Zhu, Toksöz and Burns 2008). However, due to the lack of enough knowledge of the relation between electrokinetic logs and rock physical characteristics, people still cannot extract formation information from electrokinetic logs. Thus there is an urgent need to theoretically study the variations of borehole electrokinetic wavefields with formation parameters for clarifying which parameters can be detected by electrokinetic logs.

Based on the previous studies of electrokinetic effects, Pride (1994) derived a set of governing equations, which is a combination of Biot's equations of poroelasticity and Maxwell's equations of electromagnetism, for the coupled seismic and electromagnetic fields in a homogeneous fluid-saturated porous medium. Pride and Haartsen (1996) analysed the properties of seismoelectric plane waves in the homogeneous porous medium. After this, by solving Pride's equations and using the boundary conditions on the borehole wall, Hu, Wang and Wang (2000) derived the expressions of the borehole and formation electrokinetic wavefields and simulated the full waveforms of the seismoelectric logging with an acoustic point source centred in a borehole. In their works, the dependences of the wavefield amplitudes on formation parameters (such as permeability and porosity) are compared between the seismoelectric and acoustic logs. They also investigated the influence of permeability on the time-domain wave amplitude ratio of the converted electric field to the pressure with respect to the Stoneley wave. Nevertheless this amplitude ratio changes so little with permeability that they saw no advantage of seismoelectric logging over conventional acoustic logging for permeability measurement. During the same period, by using Tang, Cheng and Toksöz (1991)'s simplified formula for the low-frequency Stoneley wave, Mikhailov, Queen and Toksöz (2000) calculated the Stoneley-wave induced electric field at quasi-static conditions and derived an approximate expression of the ratio of the electric field to the pressure (REP) in the frequency domain. It is shown from their expression that the amplitude of the REP is proportional to porosity instead of permeability. Following this, efforts have been made on the full waveform simulations of electrokinetic logs by different methods (e.g., Hu and Liu 2002; Pain *et al*. 2005; Zhan, Chi and Toksöz 2006; Hu, Guan and Harris 2007; Guan and Hu 2008). However, there are no theoretical studies on the inversion of formation permeability from electrokinetic logs.

In this paper, we propose a method to invert formation permeability by using the full waveforms of low-frequency seismoelectric logs. The method is based on the relationship of the REP's phase, which reflects the phase discrepancy between the Stoneley-wave induced electric field and the acoustic pressure, with permeability. The paper is organized as follows. Firstly, we review Pride's electrokinetic theory in porous media and the simulation of seismoelectric logs. We also investigate the sensitivity of the simulated seismoelectric logs as well as that of the REP to permeability and find that the REP's phase spectrum changes with permeability. Then we derive the frequency domain expression of the REP of the Stoneley wave in low frequencies and find that permeability is approximately in inverse proportion to the tangent of the REP's argument, which

reflects the phase discrepancy between the induced electric field and the acoustic field. Finally, we present the formula and the process for the permeability inversion and then invert permeabilities of sandstones from the simulated full waveforms of the seismoelectric logs. We also give the comparisons of the inversion values and the relative errors with those obtained by the Stoneley wave of acoustic logs in Wu *et al*. (1995).

THE SIMULATION OF ELECTROKINETIC LOGS

The electrokinetic coupling between seismic and electromagnetic wavefields in an isotropic, homogeneous fluid-saturated porous medium can be expressed as follows (Pride, 1994), assuming an $e^{-i\omega t}$ time dependence:

$$\mathbf{J} = \sigma(\omega)\mathbf{E} + L(\omega)\left(-\nabla p + \omega^2 \rho_f \mathbf{u}\right) \tag{1}$$

$$-i\omega\mathbf{w} = L(\omega)\mathbf{E} + \left(-\nabla p + \omega^2 \rho_f \mathbf{u}\right)\kappa(\omega)/\eta, \tag{2}$$

where ω is the angular frequency, t is the time, i is the imaginary unit, **E** and **J** are the electric field and the electric current density, respectively, **u** is the displacement of the solid phase, **w** is the relative displacement between the fluid and the solid phase, p is the pore fluid pressure, ρ_f and η are the density and the viscosity of the pore fluid, κ is the dynamic permeability defined by Johnson, Koplik and Dashen (1987) and σ and L are the dynamic conductivity and the electrokinetic coupling coefficient. The coupling between the seismic and electromagnetic fields is reflected in equations (1) and (2) through the terms $L(-\nabla p + \omega^2 \rho_f \mathbf{u})$ and $L\mathbf{E}$ with coefficient L. It can be seen that the pressure gradient term ∇p and the inertial force $\omega^2 \rho_f \mathbf{u}$ cause the electric current density **J** and the electric field **E** induces the filtration velocity $-i\omega\mathbf{w}$. If L is set to zero, the seismic and electromagnetic fields in the porous medium are decoupled, and Pride's equations break up into Biot's poroelastic wave equations and Maxwell's electromagnetic wave equations. The frequency dependent expression of L is given by

$$L(\omega) = L_0\left[1 - i\frac{\omega}{\omega_c}\frac{m}{4}\left(1 - 2\frac{\tilde{d}}{\Lambda}\right)^2\left(1 - i^{\frac{3}{2}}\frac{\tilde{d}}{\delta}\right)^2\right]^{-\frac{1}{2}}, \tag{3}$$

where $\omega_c = \phi\eta/\alpha_\infty \rho_f \kappa_0$ is a critical angular frequency that separates the low-frequency viscous flow from the high-frequency inertial flow, ϕ is the porosity, α_∞ is the tortuosity, κ_0 is the Darcy permeability, m is a dimensionless parameter that has little change for the majority of sedimentary rocks (Johnson, Koplik and Dashen 1987) and is assumed to be 8.0 for the sandstones in our calculation, δ is the viscous skin depth, $\Lambda = \sqrt{m\alpha_\infty\kappa_0/\phi}$ and $\tilde{d}$ are respectively the weighted volume-to-surface radio and the length that is equal to or less than the Debye length, $L_0 = -(\phi\varepsilon_f\varsigma/\alpha_\infty\eta)(1 - 2\tilde{d}/\Lambda)$ is the low-frequency limit of the electrokinetic coupling coefficient, ε_f is the permittivity of the pore fluid and ς is the electric potential at the shear plane, which separates the two layers, i.e., the adsorbed layer and the diffuse layer in the electric double layer. The expression $\varsigma = 0.008 + 0.026\log_{10}(C_f)$ given by Pride and Morgan (1991) is used in this paper, C_f is the pore fluid salinity. Note that coefficient L can be measured in the laboratory by using both the seismoelectric and electroseismic conversions of a rock core (Pengra, Li and Wong 1999; Wang *et al*. 2010).

By solving Pride's equations in the cylindrical coordinate system (r, θ, z) with the z axis being the borehole axis and the origin coinciding with the centre of the point source and using the boundary conditions on the borehole wall, we can simulate the electrokinetic logs in a fluid-filled borehole surrounded by a homogeneous fluid-saturated porous formation (e.g. Hu, Wang and Wang 2000). Note that in the seismoelectric conversion of a seismic wave inducing an electromagnetic field, the influence of the electromagnetic field on the seismic wave is weak enough and can be ignored (e.g., Hu and Liu 2002; Pain *et al*. 2005; Haines and Pride 2006). This fact allows us to calculate the seismoelectric logs simply by solving the seismic wave separately according to Biot's poroelastic wave theory and then solving the seismic-induced electromagnetic field.

Figures 1 and 2 give examples of the simulated full waveforms of the seismoelectric logs. The medium parameters are listed in Table 1. A point pressure source of a cosine wave oscillating within an envelope is employed, whose intensity is assumed to be 1.0 Pa of the peak pressure at one millimetre away from the source centre. The centre frequencies are $f_0 = 6$ kHz and $f_0 = 1$ kHz in Figs. 1 and 2, respectively. Shown in Fig. 1(a) are the waveforms of the pressure p and the z-component electric field E_z received at different locations along the borehole axis. The waveforms are normalized with respect to the peak value of the response at a location of receiver-to-source distance $z = 0.5$ m. More details at $z =$ 3.0 m are given in Fig. 1(b). There are three different wave groups in pressure waveforms (shown by lines b-b, c-c and d-d, respectively), in order of arrival time. They are the compressional, the shear and pseudo-Rayleigh and the Stoneley wave groups. In the electric field waveforms, there are three corresponding wave groups that are the stationary electric

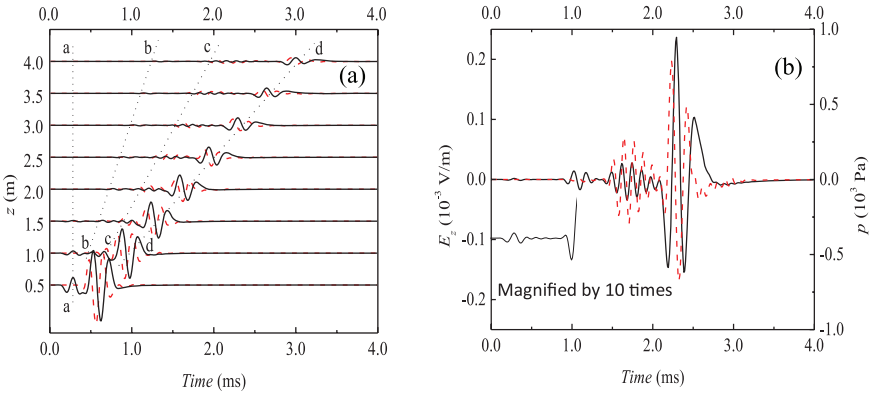

Figure 1 Full waveforms of pressure p (dashed lines) and electric field E_z (solid lines) along the borehole axis of the seismoelectric logging in a sandstone formation with 6 kHz source centre frequency. (a)z = 0.5-4.0 m, the dotted lines with a, b, c, and d denote four different wave groups in the full waveforms. (b)z = 3.0 m.

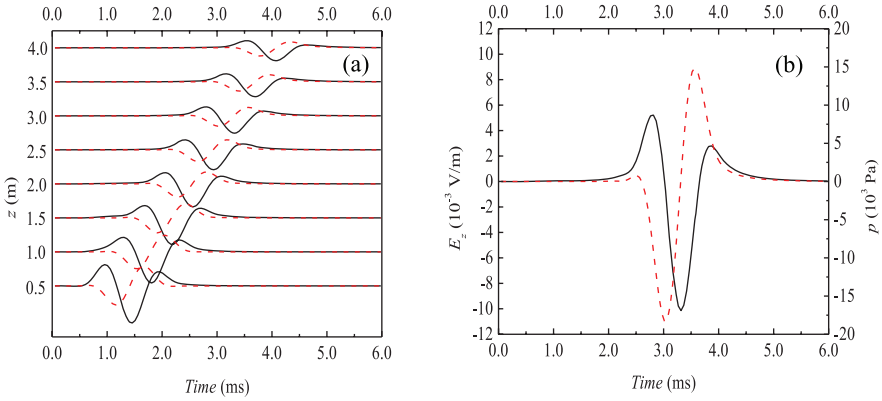

Figure 2 Full waveforms of pressure p (dashed lines) and electric field E_z (solid lines) along the borehole axis of the seismoelectric logging in a sandstone formation with 1 kHz source centre frequency. (a) z = 0.5-4.0 m (b) z = 3.0 m.

field accompanying the propagating acoustic waves, with no extent outside the acoustic pulses.

When magnifying by five times the waveforms in the first millisecond in Fig. 1, it can be seen that a wave group (shown by line a-a) arrives earlier than the compressional wave and reaches the different receivers almost at the same time. This is the independently propagating electromagnetic wave generated by acoustic waves when hitting on the borehole wall. For the waveforms excited by the source of 1 kHz centre frequency in Fig. 2, the compressional and shear waves are not very well excited, while the Stoneley wave dominates the waveforms. Employing a source of low frequencies can raise the Stoneley wave amplitude effectively. The Stoneley wave amplitudes of the pressure and its accompanied electric field in Fig. 2(b) are about 20 and 40 times larger than those in Fig. 1(b), respectively.

Because of the sensitivity of Stoneley wave attenuation to permeability, we investigate the amplitude change with permeability of the Stoneley wave and its accompanied electric field of seismoelectric logs. Table 2 shows the peak Stoneley wave amplitudes of the simulated p and E_z waveforms for sandstones with different porosities and permeabilities. The amplitudes of the REP are also calculated and listed in Table 2. These simulations are excited by a $f_0 = 1$ kHz source and received by a receiver located on the borehole axis at z = 3.0 m. The frame bulk and shear moduli of the porous formations change with porosity according to the experimental results of Vernik (1994) for sandstones. The data in Table 2 are also plotted in Fig. 3 in order to clearly show the amplitude variation with permeability. When κ_0 >1.0 millidarcy (mD), the amplitudes of both the pressure and the electric field decrease with increasing permeability. When κ_0 <1.0 mD, the pressure amplitude still decreases with increasing permeability while the electric field amplitude increases slightly. From the data in Table 2 and by comparing Fig. 3(a), (b), we find that the sen-

Table 1 Input medium parameters of seismoelectric logging

Parameter	Property	Value
ϕ	Porosity (%)	20
κ_0	Static Darcy permeability (mD)	1000
α_∞	Tortuosity	3
K_b	Frame bulk modulus (GPa)	14.39
G_b	Frame shear modulus (GPa)	13.99
K_s	Solid bulk modulus (GPa)	35.70
K_f	Pore fluid bulk modulus (GPa)	2.25
ρ_s	Solid density (kg/m^3)	2650
ρ_f,ρ_b	Pore fluid density, borehole fluid density (kg/m^3)	1000
C_f,C_b	Pore fluid salinity, borehole fluid salinity (mol/L)	0.01
σ_f,σ_b	Pore fluid conductivity, borehole fluid conductivity(S/m)	9.28×10^{-2}
η	Pore fluid viscosity (Pa·s)	10^{-3}
r_b	Borehole radius (m)	0.1
v_{ba}	Acoustic velocity in borehole fluid (m/s)	1500

sitivities of the pressure and the electric field amplitudes to permeability are almost to the same extent except when $\kappa_0 > 1.0$ darcy (D). It can also be seen from Fig. 3(c) that the REP amplitude changes slightly with permeability when $\kappa_0 < 1.0$ D but it decreases significantly when $\kappa_0 > 1.0$ D. The reason is that the change of the electric field amplitude is controlled by two mechanisms together, one is the attenuation causing the decrease of the pressure amplitude with increasing permeability and the other is the electrokinetic conversion ability reflected by coefficient L. Within the range of 1.0 mD$< \kappa_0 <$ 1.0 D, the inequalities $\tilde{d} \ll \Lambda$ and $\omega \ll \omega_c$ make the electrokinetic coupling coefficient to be $L \approx L_0 \approx -\phi\varepsilon_f\varsigma/\alpha_\infty\eta$, which is independent of permeability. Thus the variation of the electric field corresponds with that of the pressure. Within the extreme low-permeability range of $\kappa_0 <$1.0 mD, the length $\Lambda = \sqrt{m\alpha_\infty\kappa_0/\phi}$ is so small that inequality $\tilde{d} \ll \Lambda$ is invalid and coefficient L is smaller than $-\phi\varepsilon_f\varsigma/\alpha_\infty\eta$, which causes the electric field to decrease even as pressure increases. Within the extreme high-permeability range of $\kappa_0 >$1.0 D, the critical angular frequency $\omega_c = \phi\eta/\alpha_\infty\rho_f\kappa_0$ is so small that inequality $\omega \ll \omega_c$ is invalid and coefficient L is also smaller than $-\phi\varepsilon_f\varsigma/\alpha_\infty\eta$, thus the decrease of the electric field is more than that of the pressure.

Comparing Fig. 3(a), (b), we find that the amplitude change of the electric field with porosity is also different from that of the pressure. It can be seen from Fig. 3(a) that the amplitude of the pressure decreases monotonically with increasing porosity, because the moduli and the wave speed decrease while the attenuation increases for a higher pore formation. It can be seen from Fig. 3(b) and the data in Table 2 that the amplitude of the electric field increases with increasing porosity for common permeabilities but it changes to decrease with porosity for the extreme high-permeability $\kappa_0 = 10$ D. This is because of the two mechanisms mentioned above. Within the range of $\kappa_0 < 1.0$ D, the electrokinetic conversion mechanism dominates the amplitude change of the electric field and the increase of coefficient L with porosity causes the electric field to increase even as pressure decreases. When permeability reaches 10 D, the pressure attenuation dominates the amplitude change of the electric field and thus the electric field decreases with porosity. There is a critical permeability where the amplitude of the electric field is invariant with porosity. It can be seen from Fig. 3(b) that the three broken lines for different porosities intersect with each other at permeability between 1.0 D and 10 D. Because the electric field increases while the pressure decreases with increasing porosity except for extreme high-permeability formations, the amplitude of the REP is more sensitive to porosity than that of the pressure or the electric field. The significant dependence shown in Fig. 3(c) of the REP amplitude on porosity but not per-

Table 2 The peak Stoneley wave amplitudes of pressure p, electric field E_z and the ratio of the converted electric field to the pressure for different porosities and permeabilities

	$\phi = 10$ (%)			$\phi = 20$ (%)			$\phi = 30$ (%)		
κ_0 (mD)	p (kPa)	E_z (mV/m)	REP (μV/Pa·m)	p (kPa)	E_z (mV/m)	REP (μV/Pa·m)	p (kPa)	E_z (mV/m)	REP (μV/Pa·m)
0.1	48.25	15.87	0.329	46.77	22.88	0.489	43.10	25.93	0.602
1	47.72	16.32	0.342	46.07	23.96	0.520	42.42	27.64	0.652
10	46.02	15.89	0.345	43.83	23.15	0.528	40.25	26.77	0.665
100	40.32	13.81	0.343	37.09	19.49	0.526	33.34	21.91	0.657
10^3	24.00	7.76	0.323	19.81	9.80	0.495	17.12	10.48	0.612
10^4	7.44	1.45	0.194	2.647	0.71	0.267	1.50	0.42	0.279

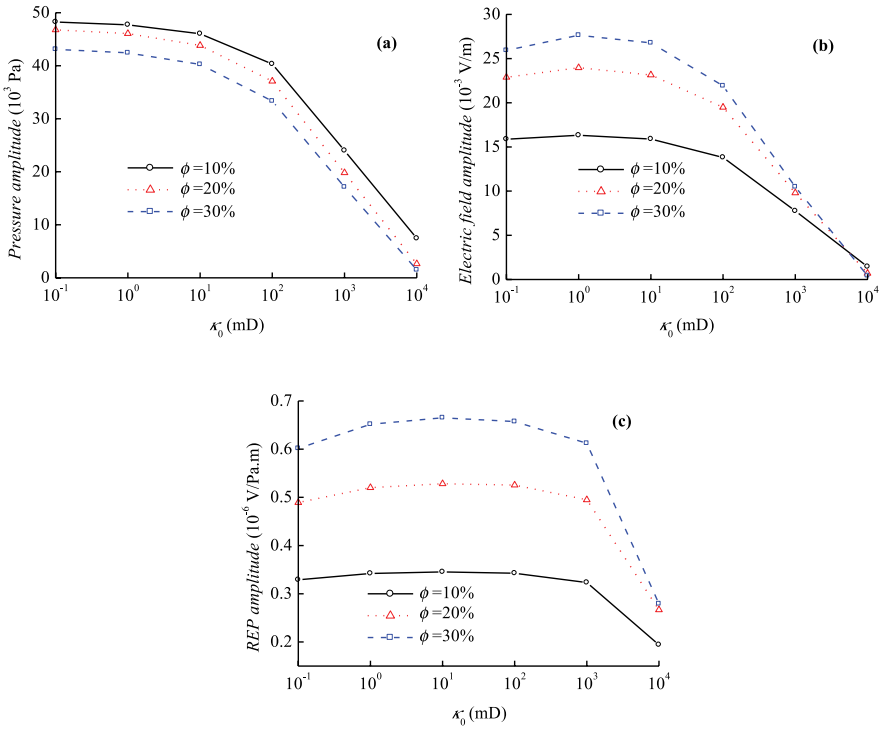

Figure 3 Amplitude variations of the pressure, the electric field and the REP with different porosities and permeabilities, according to the data in Table 2. (a) the pressure (b) the electric field (c) the REP.

meability agrees with the proportional relationship between the REP amplitude and porosity derived by Mikhailov, Queen and Toksöz (2000).

As we see no notable advantage to invert formation permeability from the amplitude of the electric field or the REP of the seismoelectric logs, which differs from the viewpoint of Singer *et al*. (2005), we further investigate the phase spectrum of the REP in the frequency domain. Shown in Fig. 4 are the frequency-dependent curves of the tangent of the Stoneley wave REP's argument for different permeabilities of sandstones. These curves are obtained by using the method of analysing individual arrivals in well logs that is extended from that for acoustic logs (Kurkjian 1985). Firstly we obtain the Stoneley waves in the frequency domain from the residue calculations of the borehole pressure and electric field functions at the Stoneley wave pole $k = k_{st}$, where k is the axial wavenumber and k_{st} is the wavenumber of the Stoneley wave. We then obtain the frequency-dependent REP by dividing the electric field by the pressure. Finally, we obtain the tangent of REP's argument by dividing the REP's imaginary part by its real part. The detailed process of these calculations is given in Wang (2010) and Wang, Hu and Guan (2012). The REP's argument reflects the phase discrepancy between the electric field and the pressure. In Fig. 4 the tangents of the REP's argument are identically negative at all frequencies, indicating that the phase of the electric field always lags behind that of the pressure. This finding agrees with the display of the full waveforms in Fig. 2. It is seen from Fig. 4

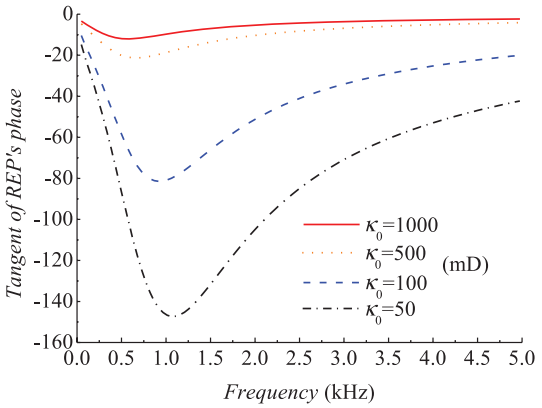

Figure 4 Frequency-dependent curves of the tangent of the REP's phase for different permeabilities of sandstones obtained from the residue calculations of the borehole pressure and electric field functions at the Stoneley wave pole.

that for a given permeability the tangent curve looks like a valley, and the absolute value of the tangent increases firstly with frequency, reaches a maximum value at the bottom point of the valley, and then decreases with frequency. Comparing the tangent curves for different permeabilities, it is seen that the frequency of this bottom point becomes smaller with the increase of permeability. The tangent of REP's phase changes with permeability: the larger the permeability, the smaller the absolute value of the tangent. It is found that the tangent of REP's phase is very sensitive to permeability. For example, the tangent at 1.0 kHz changes more than eight times from -9.64 to -80.79 when permeability decreases ten times from 1.0 D to 0.1 D.

THE RELATION BETWEEN THE THE RATIO OF THE CONVERTED ELECTRIC FIELD TO THE PRESSURE'S PHASE AND PERMEABILITY

In order to analyse the relation between the REP's phase and permeability quantitatively, the frequency-dependent expression of the REP with respect to the low-frequency ($\omega < \omega_c$) Stoneley wave of seismoelectric logs is derived as

$$R_{EP}(\omega) = i\frac{\phi\varepsilon_f\varsigma}{\eta\alpha_\infty}\left(1 - \frac{m}{8}\frac{-i\omega}{\omega_c}\right)R_I. \tag{4}$$

This equation was first given by Plyshchenkov and Nikitin (2010). Nevertheless, we find that an approximation used in their deducing process is unreasonable for high-porosity and low-permeability formations whose pores have too much clay. A detailed derivation and explanation of equation (4) and the expression of $R_I$are given in Appendix A. The expression of the REP has a similar form as that given by Mikhailov, Queen and Toksöz (2000), who derived by using the quasi-static electromagnetic condition and Tang, Cheng and Toksöz (1991)'s approximate formula of the low-frequency Stoneley wave. As a result, their expression of R_I is different from that in this paper.

Calculating the term R_I in equation (4) by employing the parameters in Table 1, we find that the real part of R_I is much larger than the imaginary part if the frequency is more than 500 Hz. Further calculations show that the real part of R_I is always much larger than the imaginary part for various formations if the frequency is more than 500 Hz. Hence similar to that in Plyshchenkov and Nikitin (2010), we can approximately consider the term R_I as a real function and then obtain the following expression from equation (4).

$$\tan(\theta_{EP}) = \frac{\mathrm{Im}(R_{EP})}{\mathrm{Re}(R_{EP})} \approx -\frac{\omega_c}{\omega} = -\frac{\phi\eta}{2\pi f\alpha_\infty\rho_f\kappa_0}. \tag{5}$$

where θ_{EP} denotes the arguments of the REP and their principal value is the REP's phase, Im and Re denote the imaginary and real parts, respectively and f is the frequency. Compared with the equation of the ratio of the real part to the imaginary part of the REP in Plyshchenkov and Nikitin (2010), equation (5) has explicit physical meaning to show the relations between the REP's phase and some parameters of porous formations. It is seen that the absolute value of $\tan(\theta_{EP})$ is approximately in inverse proportion to frequency (f),tortuosity (α_∞),permeability (κ_0) and pore fluid density (ρ_f) and in direct proportion to porosity (ϕ) and pore fluid viscosity (η). To the right of the bottom point of each curve in Fig. 4, the absolute value of $\tan(\theta_{EP})$ decreases with frequency, this agrees with the inverse proportion of the absolute value of $\tan(\theta_{EP})$ to the frequency shown in equation (5). In addition, we have calculated from Fig. 4 that the absolute value of $\tan(\theta_{EP})$ at a frequency higher than that at the bottom point increases more than eight times when permeability reduces ten times from 1.0 D to 0.1 D. This result is in general accord with the inverse proportion of the absolute value of $\tan(\theta_{EP})$ to the permeability shown in equation (5). Thus the value of $\tan(\theta_{EP})$ at a frequency higher than that at the bottom point in Fig. 4 should be used when we invert permeability based on the relationship between $\tan(\theta_{EP})$ and permeability.

THE PERMEABILITY INVERSION FROM SEISMOELECTRIC LOGS

Rewriting equation(5), we obtain the permeability inversion formula as

$$\kappa_0 = -\frac{\phi\eta}{2\pi f\cdot\alpha_\infty\rho_f\cdot\tan(\theta_{EP})}. \tag{6}$$

Based on equation (6), we propose the permeability inversion method by using the tangent of REP's phase obtained from the low-frequency seismoelectric logs. The detailed inversion process is as follows. 1) Fourier transforming the received pressure and electric field signals at the same location in the borehole to obtain the frequency-dependent REP and then dividing the imaginary part of the REP by the real part to make the curve of $\tan(\theta_{EP})$. An acoustic transmitter with a centre frequency between 0.5 -2 kHz is employed as the source of the seismoelectric logging. The reason is that the full waveforms at these frequencies are dominated by the Stoneley wave, which is dependent on permeability. In addition, using

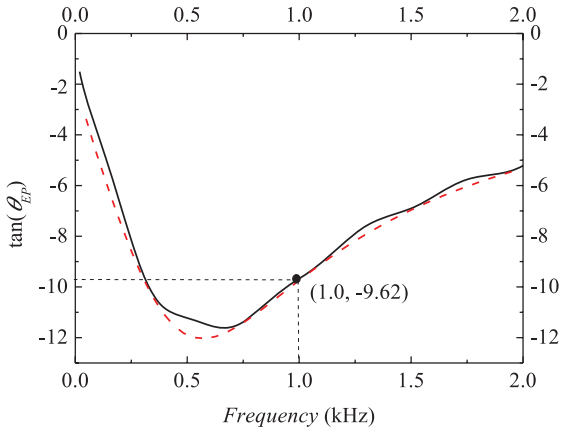

Figure 5 Comparison of the tangent of the REP's phase obtained from the simulated full waveforms in Fig. 2(b) (solid line) with that obtained from the residue calculation method (dashed line).

a source with lower frequencies can improve the ability of electrokinetic conversion and induce stronger electric signals due to the inverse proportion of the amplitude of coefficient $L(\omega)$ to frequency. Figure 5 gives an example of the curve of $\tan(\theta_{EP})$ obtained from the simulated full waveforms in Fig. 2(b) for permeability of 1.0 D and compares it with that obtained from the residue calculation method. 2) According to equation (6), if porosity, tortuosity and pore fluid properties (density and viscosity) have been measured by some method or estimated by empirical formulas, permeability can be evaluated by using a certain value and the corresponding frequency of $\tan(\theta_{EP})$ from the curve segment where frequencies are higher than that at the bottom point. For example, using $\tan(\theta_{EP}) = -9.62$ at 1.0 kHz in Fig. 5 we calculate the inverted permeability of 1.1 D and an error of 10% relative to the value used in the simulation.

As listed in Table 3 the permeabilities of different porous formations are inverted and compared with the values used in the simulation. The sources with $f_0 = 2$ kHz and $f_0 = 0.5$ kHz centre frequencies are respectively employed, in order to investigate the effect of the source frequency on the inversion. It is assumed that the pore fluid properties of the different formations are the same as those in Table 1, i.e., the density and viscosity are $\rho_f = 1000$ kg/m^3 and $\eta = 10^{-3}$ Pa·s. The porosities and permeabilities used in Table 3 are the same as those used in Wu *et al.* (1995), so that we can compare the accuracy of the permeability inversion from the seismoelectric logs with that from the acoustic logs. Because the curves of $\tan(\theta_{EP})$ with respect to the Stoneley wave are approximately obtained from the full waveforms, some fluctuations emerged in the curves (see Fig. 5) caused by other wave groups in the full waveforms. In order to reduce this influence and obtain more reliable inversion results, the inverted permeabilities in Table 3 are averaged by those calculated from different frequencies higher than the centre frequency.

It is seen from Table 3 that the relative error is larger in high-porosity and low-permeability formations. The reasons are as follows. When porosity is fixed, the minor term $\phi/r_b Y_{pf} \alpha_\infty \eta_{ba}$, which is neglected during the derivation of the permeabil-

Table 3 Comparisons between the inverted permeabilities and the permeabilities used in simulation for different sandstone formations

Porosity $\phi = 8.5\%$, Tortuosity $\alpha_\infty = 12$											
Permeabilities used in simulation (mD)		6	8	10	20	40	80	160	320	640	800
$f_0 = 2$ kHz	Inverted permeabilities (mD)	5.92	7.95	9.97	20.0	39.7	77.0	139	218	288	306
	Relative errors (%)	−1.3	−0.6	−0.3	0.0	−0.8	−3.8	−13.1	−31.9	−55.0	−61.8
$f_0 = 0.5$ kHz	Inverted permeabilities (mD)	13.2	14.9	16.7	25.9	44.7	82.5	158	301	540	635
	Relative errors (%)	120	86.3	67.0	29.5	11.8	3.1	−1.3	−5.9	−15.6	−20.6
Porosity $\phi = 12.5\%$, Tortuosity $\alpha_\infty = 8$											
Permeabilities used in simulation (mD)		10	20	40	80	160	320	640	800	1000	1200
$f_0 = 2$ kHz	Inverted permeabilities (mD)	9.4	19.6	39.8	79.6	155	285	457	513	565	605
	Relative errors (%)	−6.0	−2.0	−0.5	−0.5	−3.1	−10.9	−28.6	−35.9	−43.5	−49.6
$f_0 = 0.5$ kHz	Inverted permeabilities (mD)	13.7	22.4	40.3	77.5	153	303	592	727	886	1031
	Relative errors (%)	37.0	12.0	0.8	−3.1	−4.4	−5.3	−7.5	−9.1	−11.4	−14.1
Porosity $\phi = 16.5\%$, Tortuosity $\alpha_\infty = 6$											
Permeabilities used in simulation (mD)		6	8	20	40	60	100	500	800	1400	2000
$f_0 = 2$ kHz	Inverted permeabilities (mD)	4.6	6.8	19.3	40.0	60.4	101	459	655	907	1052
	Relative errors (%)	−23.3	−15	−3.5	0.0	0.7	1.0	−8.2	−18.1	−35.2	−47.4
$f_0 = 0.5$ kHz	Inverted permeabilities (mD)	11.3	13.5	26.0	46.0	65.9	105	498	783	1319	1795
	Relative errors (%)	88.3	68.8	30.0	15.0	9.8	5.0	−0.4	−2.1	−5.8	−10.3

ity inversion formula (see equation (A-22) in Appendix A), becomes larger with the decrease of permeability. Thus the inversion errors are relatively large for low-permeability formations, especially for high-porosity and low-permeability formations whose pores are blocked up by mud. Even so, for low-permeability formations, the inversion errors of using the seismoelectric logs are smaller than those of using the acoustic logs. To the other extreme, in formations with very low critical frequency, which is typical of low-porosity and high-permeability formations, the inversion error may be caused by the relatively high frequency at which the inertial force dominates the pore fluid flow. When we derive the REP, the expressions of $L(\omega)$ and $\kappa(\omega)$ are simplified by the Taylor series at $\omega = 0$. If the differences between $L(\omega)$ and L_0 and that between $\kappa(\omega)$ and κ_0 increase, the errors in the simplifications of $L(\omega)$ and $\kappa(\omega)$ become larger and cause a larger difference between the left- and right-hand sides of equation (5) and thus a larger inversion error. With the increase of permeability the critical angular frequency $\omega_c = \phi\eta/\alpha_\infty\rho_f\kappa_0$ becomes smaller, thus the angular frequency ω used to invert permeability is closer to or even larger than ω_c. As a result, compared with L_0 and κ_0 in the low-frequency limit, the amplitudes of $L(\omega)$ and $\kappa(\omega)$ decrease and the phases of them increase due to the larger high-frequency inertial force. For example, if the permeability is $\kappa_0 = 10$ D (other medium parameters are the same as those in Table 1) and the frequency used for inversion is $f = 2$ kHz, the absolute value of $\tan(\theta_{EP})$ calculated from equation (5) is about one half of that obtained from the waveforms. Therefore the relative errors are relatively large for high-permeability formations, especially for low-porosity and high-permeability formations whose fractures are developed and the solid matrix is compact. For ordinary formations between the above two extremes, the permeability inversion errors are small.

From the comparison of the permeabilities inverted by employing the $f_0 = 0.5$ kHz and $f_0 = 2$ kHz sources in Table 3, we find that the relative errors of using the higher frequency are much smaller for low-permeability formations. The reason is that the neglected minor term $\phi/r_b Y_{pf}\alpha_\infty\eta_{ba}$ decreases with the increase of frequency. The inversion errors of using the lower frequency are much smaller for high-permeability formations. With the decrease of angular frequency ω the high-frequency inertial force reduces, thus the differences between $L(\omega)$ and L_0 and between $\kappa(\omega)$ and κ_0 decrease. If the permeability is $\kappa_0 = 10$ D and the frequency used for the inversion is $f = 0.5$ kHz, the absolute value of $\tan(\theta_{EP})$ calculated from equation (5) is about only 14.8% smaller than that obtained from the waveforms.

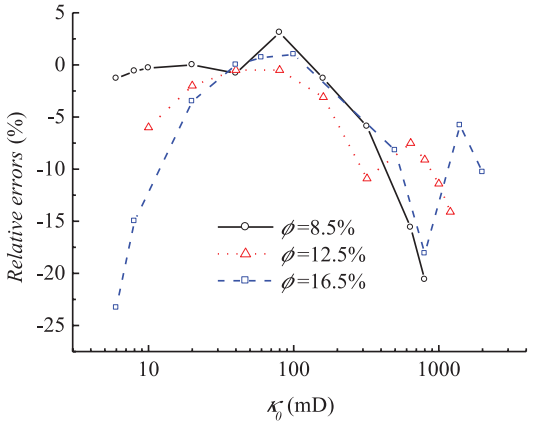

Figure 6 Relative errors in the permeability inversion by using the tangents of the REP's phase of the seismoelectric logs, according to the data in Table 3 and after correction.

Based on the above analysis of the errors, the inversion process is modified as follows. Firstly we calculate a reference permeability κ_{re} by using the known formation porosity ϕ, according to the Kozeny-Carman relation that provides a way to estimate the permeability of a porous medium in terms of porosity, surface area, and grain size. The modified Kozeny-Carman relation $\kappa_{re} = B(\phi - \phi_c)^3 d^2$ given by Mavko and Nur (1997) is used, in which constant B is a geometric factor, d is the grain size and ϕ_c is a threshold porosity that depends on pore geometry. We choose $B = 5$ and $\phi_c = 2.5\%$ as those in Mavko and Nur (1997) for the sandstone with a typical grain size of $d = 250$ microns. Then we invert permeability from the seismoelectric logs excited by a $f_0 = 2$ kHz source. If the result is less than the reference permeability κ_{re}, it is regarded as the inverted permeability; otherwise if the result approaches to or is greater than κ_{re}, we invert permeability again by employing a $f_0 = 0.5$ kHz source and regard the new result as the inverted permeability. For example when porosity is $\phi = 8.5\%$, the reference permeability is calculated as $\kappa_{re} = 67.5$ mD. Thus the values less than 67.5 mD at $f_0 = 2$ kHz and the values greater than 67.5 mD at $f_0 = 0.5$ kHz in Table 3 are considered as the inverted permeabilities. According to the data in Table 3, the error distribution after modifying the inversion process is drawn in Fig. 6. It is seen that the relative errors of using the seismoelectric logs are controlled below 25%. For comparison, the error distribution of using the acoustic logs is drawn in Fig. 7 according to the data given by Wu *et al.* (1995). Note that in their works the relative errors for porosity of $\phi = 16.5\%$ and permeabilities of $\kappa_0 = 6$ mD and $\kappa_0 = 8$ mD are so big (490% and 397%) that they are not drawn in Fig. 7. From the comparison between Figs. 6 and

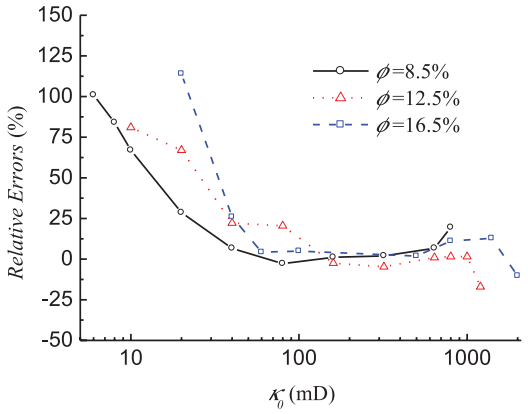

Figure 7 Relative errors in the permeability inversion by using the Stoneley wave of the acoustic logs, according to the data in Wu *et al.* (1995).

7, it is seen that the errors of using the seismoelectric logging method proposed in this paper are less than those of using the acoustic logging method, especially for low-permeability formations.

DISCUSSION

The theoretical calculation and analysis mentioned above of inverting permeability from the REP's phase have shown the possibility of applying seismoelectric logs to estimate formation permeability in the future. Note that the present inversion method is based on the premise that porosity, tortuosity and pore fluid properties are known. In general, porosity can be accurately obtained by using acoustic logging or other methods. If formation porosity is known, tortuosity can be approximated to $\alpha_\infty = 1/\phi$ by substituting $F = \alpha_\infty/\phi$ (Brown 1980) into Archie's empirical formula $F = 1/\phi^2$ (Archie, 1942), where F is the formation factor. In addition, F can be measured by using the electric logging method. If F is known, tortuosity as well as porosity need not to be known before permeability inversion. Even though the pore fluid viscosity is unknown, the present method can still be used to calculate the mobility, i.e., the ratio of permeability to viscosity. The mobility reflects the fluid movement under the unit pressure gradient in porous formations and is one of the key indexes for comprehensive evaluation of oil and gas reservoirs.

In the present method, the frequency-dependent curve of the REP's phase is needed by Fourier transforming the time-domain waveforms. Because the REP's phase reflects the Stoneley-wave phase discrepancy between the electric field and the pressure, it will simplify the inversion process if this phase discrepancy that was measured directly from the time-domain waveforms can be used for inversion. Our theoretical calculation (Wang, 2010; Wang, Hu and Guan 2012) shows that the average change of the phase at 3.0 kHz with permeability is about 0.155 degrees per 10 mD when permeability is between 200 mD and 800 mD. Even if permeability is between 1 mD and 100 mD, the average change of the phase at 3.0 kHz with permeability is about 0.181 degrees per 10 mD. This indicates that the REP's phase is still sensitive to permeability for low-permeable formations. Nevertheless the sample interval of common logging instruments is about 20 points per one wavelength, so that the resolution of the phase discrepancy is on the order of 1.0 degree. Thus for obtaining a permeability-sensitive phase discrepancy, the sampling-point number should be increased greatly.

When investigating the relation between REP's phase and permeability and inverting permeabilities in this paper, the formations are considered as homogeneous porous media. In actual logging situations, however, the formation is commonly stratified and there is a mud cake layer nearby the borehole wall. Their effects on the accuracy of the present method should be investigated in the future. This work can be implemented by using the numerical method, such as finite-element and finite-difference, to simulate waveforms of these situations and then inverting permeabilities from the waveforms. Furthermore, the relation proposed in this paper is based on Pride's electrokinetic theory in which some assumptions are used (Pride 1994) and the permeability inversion in this paper is implemented by using theoretically simulated waveforms. Thus permeability inversion from the borehole seismoelectric signals measured in the laboratory or field is necessary in future work.

CONCLUSIONS

In this paper, we have theoretically studied the relation between seismoelectric logs and formation permeability and proposed a permeability inversion method. For porous formations with different permeabilities, the changes of the Stoneley wave amplitudes of both the pressure and the converted electric field are almost to the same extent except for extremely high-permeability formations, thus we see no notable advantage to invert permeability by using the converted electric field amplitude.

We have investigated the changes of both the amplitude and phase of the Stoneley wave the ratio of the converted electric field to the pressure for formations with different porosities and permeabilities. It is found that the REP's am-

plitude is sensitive to porosity rather than permeability, while the REP's phase that reflects the phase discrepancy between the electric field and the pressure is sensitive to permeability. We have derived the frequency-dependent expression of the Stoneley wave REP and found that the tangent of the REP's phase is approximately in inverse proportion to the frequency, the tortuosity, the permeability and the pore fluid density and in direct proportion to the porosity and the pore fluid viscosity.

We have inverted the permeabilities of different sandstone formations. The relative errors after modification are controlled below 25% for different porosities and permeabilities. Compared with the inverted permeabilities of the acoustic logging method, those of using the seismoelectric logging presented in this paper are closer to the values used in simulation.

ACKNOWLEDGEMENTS

This work is supported by the National Natural Science Foundations of China (40874062 and 41174110), Special Research Funds of Seismology in China (200808072), Natural Science Foundation of Heilongjiang Province of China (QC2010025), Research Fund for the Doctoral Program of Higher Education of China (20102302120024), Postdoctoral Science Foundation of China (2011M500651), Fundamental Research Funds for the Central Universities (HIT. NSRIF. 2010071) and the Research Fund of Heilongjiang Provincial Education Department (11551363). The authors are very grateful to Zhenya Zhu and Tobias Müller for their revision suggestions for this paper.

REFERENCES

Abramowitz M. and Stegun I.A. 1965. Handbook of mathematical functions with formulas, graphs, and mathematical tables. Dover Publications Inc., Mineola, N.Y.

Archie G.E. 1942. The electrical resistivity log as an aid in determining some reservoir characteristics. *Transactions of the American Institute of Mechanical Engineers* **146**, 54–62.

Biot M.A. 1956a. Theory of propagation of elastic waves in a fluid-saturated porous solid. I-Low-frequency range. *Journal of the Acoustical Society of America* **28**, 168–178.

Biot M.A. 1956b. Theory of propagation of elastic waves in a fluid-saturated porous Solid. II-Higher-frequency range. *Journal of the Acoustical Society of America* **28**, 178–191.

Biot M.A. 1962. Mechanics of deformation and acoustic propagation in porous media. *Journal of Applied Physics* **33**, 1482–1498.

Brown R.J.S. 1980. Connection between formation factor for electrical resistivity and fluid-solid coupling factor in Biot's equations for acoustic waves in fluid-filled porous media. *Geophysics* **45**, 1269–1275.

Cheng C.H., Zhang J.Z. and Daniel R.B. 1987. Effects of in-situ permeability on the propagation of Stoneley (tube) waves in a borehole. *Geophysics* **52**, 1279–1289.

Frenkel J. 1944. On the theory of seismic and seismoelectric phenomena in a moist soil. *Journal of Physics* (in Russian) **8**, 230–241.

Guan W. and Hu H.S. 2008. Finite-difference modeling of the electroseismic logging in a fluid-saturated porous formation. *Journal of Computational Physics* **227**, 5633–5648.

Guan W., Hu H.S. and Chu Z.T. 2006. Formulation of the acoustically-induced electromagnetic field in a porous formation in terms of Hertz vectors and simulation of the borehole electromagnetic field excited by an acoustic multipole source. *Acta Physica Sinica* (in Chinese) **55**, 267–274.

Haines S.S. and Pride S.R. 2006. Seismoelectric numerical modeling on a grid. *Geophysics* **71**, N57–N65.

Hu H.S., Guan W. and Harris J.M. 2007. Theoretical simulation of electroacoustic borehole logging in a fluid-saturated porous formation. *Journal of the Acoustical Society of America*. **122**, 135–145.

Hu H.S. and Liu J. 2002. Simulation of the converted electric field during acoustoelectric logging. 72nd SEG Annual International Meeting, Salt Lake City, Utah, USA, Expanded Abstracts, **21**, 348–351.

Hu H.S., Wang K.X. and Wang J.N. 2000. Simulation of acoustically induced electromagnetic field in a borehole embedded in a porous formation. Borehole Acoustics Annual Report, Earth Resources Laboratory, Massachusetts Institute of Technology 13, 1–13.30.

Hunt C.W. and Worthington M.H. 2000. Borehole electrokinetic responses in fracture dominated hydraulically conductive zones. Geophysical Research Letters. **27**, 1315–1318.

Ivanov A.G. 1939. Effect of electrization of earth layers by elastic waves passing through them. *Doklady Akademii Nauk SSSR* (in Russian) **24**, 42–45.

Johnson D.L., Koplik J. and Dashen R. 1987. Theory of dynamic permeability and tortuosity in fluid-saturated porous media. *Journal of Fluid Mechanics* **176**, 379–402.

Kurkjian A.L. 1985. Numerical computation of individual far-field arrivals excited by an acoustic source in a borehole. *Geophysics* **50**, 852–866.

Mavko G. and Nur A. 1997. The effect of a percolation threshold in the Kozeny-Carman relation. *Geophysics* **62**, 1480–1482.

Mikhailov O.V., Queen J. and Toksöz M.N. 2000. Using borehole electroseismic measurements to detect and characterize fractured (permeable) zones. *Geophysics* **65**, 1098–1112.

Morgan F.D., Williams E.R. and Madden T.R. 1989. Streaming potential properties of westerly granite with applications. *Journal of Geophysical Research* **94**, 12449–12461.

Pain C.C., Saunders J.H., Worthington M.H. *et al*. 2005. A mixed finite-element method for solving the poroelastic Biot equations with electrokinetic coupling. *Geophysical Journal of International* **160**, 592–608.

Pengra D.B., Li S.X. and Wong P.Z. 1999. Determination of rock properties by low-frequency AC electrokinetics. *Journal of Geophysical Research* **104**, 29485–29508.

Plyshchenkov B.D. and Nikitin A.A. 2010. Borehole acoustic and electric Stoneley waves and permeability. *Journal of Computational Acoustics* **18**, 87–115.

Pride S.R. 1994. Governing equations for the coupled electromagnetics and acoustics of porous media. *Physical Review B* **50**, 15678–15696.

Pride S.R. and Haartsen M.W. 1996. Electroseismic wave properties. *Journal of the Acoustical Society of America* **100**, 1301–1315.

Pride S.R. and Morgan F. 1991. Electrokinetic dissipation induced by seismic waves. *Geophysics* **56**, 914–925.

Rosenbaum J.H. 1974. Synthetic microseismograms: Logging in porous formations. *Geophysics* **39**, 14–32.

Singer J., Saunders J., Holloway L. *et al.* 2005. Electrokinetic logging has the potential to measure permeability. *46th SPWA Annual Logging Symposium*, New Orleans, Louisiana, United States

Tang X.M. and Cheng C.H. 1996. Fast inversion of formation permeability from Stoneley wave logs using a simplified Biot-Rosenbaum model. *Geophysics* **61**, 639–64.

Tang X.M., Cheng C.H. and Toksöz M.N. 1991. Dynamic permeability and borehole Stoneley waves: A simplified Biot-Rosenbaum model. *Journal of the Acoustical Society of America* **90**, 1632–1646.

Tsang L. and Rader D. 1979. Numerical evaluation of the transient acoustic waveform due to a point source in a fluid-filled borehole. *Geophysics* **44**, 1706–1720.

Vernik L. 1994. Predicting lithology and transport properties from acoustic velocities based on petrophysical classification of siliclastics. *Geophysics* **59**, 420–427.

Wang J, Hu H.S. and Xu X.R. et al. 2010. Experimental measurement study on rock permeability based on the electrokinetic effect. *Chinese Journal of Geophysics* (in Chinese) **53**, 1953–1960.

Wang Z. 2010. Component wave analysis of borehole seismoelectric wavefields in a porous formation. *Thesis for the Master Degree of Harbin Institute of Technology* (in Chinese).

Wang Z. Hu H. and Guan W. 2012. Component wave analysis of the relation between borehole seismoelectric wavefields and formation permeability, accepted by *Acta Physica Sinica* (in Chinese).

Williams D.M., Zemanek J., Angona F.A. *et al.* 1984. The long spaced acoustic logging tool. *25th SPWA Annual Logging Symposium*, Paper T.

Winkler K.W., Liu H.L. and Johnson D.L. 1989. Permeability and borehole Stoneley waves: Comparison between experiment and theory. *Geophysics* **54**, 66–75.

Wu X.Y., Wang K.X., Guo L. *et al.* 1995. Inversion of permeability from the full waveform acoustic logging data. *Chinese Journal of Geophysics* (in Chinese) **38**(Suppl.I), 224–231.

Zhan X. Chi S. and Toksöz M.N. 2006. Simulation of the converted electric field during multipole logging while drilling (LWD). 76th SEG Annual International Meeting, New Orleans, Louisiana, USA, Expanded Abstracts, **25**, 446–450.

Zhu Z., Haartsen M.W. and Toksöz M.N. 1999. Experimental studies of electrokinetic conversions in fluid-saturated borehole models. *Geophysics* **64**, 1349–1356.

Zhu Z. and Toksöz M.N. 2003. Crosshole seismoelectric measurements in borehole models with fractures. *Geophysics* **68**, 1519–1524.

Zhu Z. and Toksöz M.N. 2005. Seismoelectric and seismomagnetic measurements in fractured borehole models. *Geophysics* **70**, F45–F51.

Zhu Z., Toksöz M.N. and Burns D.R. 2008. Electroseismic and seismoelectric measurements of rock samples in a water tank. *Geophysics* **73**, E153–E164.

APPENDIX A

According to the residue calculation method of analysing individual arrivals in well logs (Kurkjian 1985), the Stoneley wave REP can be expressed as

$$R_{EP}(\omega) = \frac{\mathrm{Res}(E_{zb}(r_0, k_{st}, \omega))}{\mathrm{Res}(p_b(r_0, k_{st}, \omega))}, \tag{A1}$$

where Res denotes the residue function, p_b and E_{zb} are the borehole pressure and axial electric field component, respectively, of the seismoelectric logging excited by an acoustic point source and, r_0 is the offset from the receivers to the borehole axis. The frequency-wavenumber dependent formulas of p_b and E_{zb} obtained by ignoring the effect of the electromagnetic field on the acoustic field are given by (Guan, Hu and Chu 2006),

$$p_b(r, k, \omega) = \omega^2 \rho_b \left[A_{ba} I_0(\eta_{ba} r) + 2K_0(\eta_{ba} r) \right], \tag{A2}$$

$$E_{zb}(r, k, \omega) = -\eta_{be}^2 I_0(\eta_{be} r_b) A_{be}, \tag{A3}$$

where $\eta_{ba} = \sqrt{k^2 - k_{ba}^2}$ and $\eta_{be} = \sqrt{k^2 - k_{be}^2}$ are the radial wave numbers, k_{ba} and k_{be} are the wave numbers of the electromagnetic and acoustic waves in the borehole fluid and I_0 and K_0 are modified Bessel functions of zero order.

The undetermined coefficient A_{ba} in equation (A2) can be solved from the following equations established by using the acoustic fields in the borehole and formation and the boundary conditions of the acoustic field on the borehole wall.

$$\begin{aligned} &-\eta_{ba} r_b C_1 x_1 - \left(1 + \alpha_{pf}\right) x_2 - \left(1 + \alpha_{ps}\right) x_3 - \left(1 + \alpha_s\right) x_4 \\ &\quad = -2\eta_{ba} r_b K_1(\eta_{ba} r_b), \end{aligned} \tag{A4}$$

$$\begin{aligned} &\omega^2 \rho_b \frac{r_b^2}{2G} C_2 x_1 + \left(-\frac{b_1 k_{pf}^2}{2G} + k^2 \right) r_b^2 Y_{pf} x_2 \\ &\quad + \left(-\frac{b_2 k_{ps}^2}{2G} + k^2 \right) r_b^2 Y_{ps} x_3 \\ &\quad + \left[(\eta_s r_b)^2 Y_s + \frac{k_s^2}{2k^2} \right] x_4 = -\omega^2 \rho_b \frac{r_b^2}{2G} \cdot 2K_0(\eta_{ba} r_b), \end{aligned} \tag{A5}$$

$$x_2 + x_3 + \left(1 - \frac{k_s^2}{2k^2}\right) x_4 = 0, \tag{A6}$$

$$\omega^2\rho_b\frac{r_b^2}{2G}C_2x_1+\left(-\frac{a_1k_{pf}^2}{2G}+k^2\right)r_b^2Y_{pf}x_2 + \left(-\frac{a_2k_{ps}^2}{2G}+k^2\right)r_b^2Y_{ps}x_3=-\omega^2\rho_b\frac{r_b^2}{2G}\cdot 2K_0(\eta_{ba}r_b). \tag{A7}$$

where $x_1=A_{ba}$, $x_2=\eta_{pf}r_bK_1(\eta_{pf}r_b)A_{pf}$, $x_3=\eta_{ps}r_bK_1(\eta_{ps}r_b)A_{ps}$, $x_4=ik\eta_sr_bK_1(\eta_sr_b)A_s$, $C_2=I_0(\eta_{ba}r_b)$, $Y_l=K_0(\eta_lr_b)/\eta_lr_bK_1(\eta_lr_b)$, $(l=pf,ps,s)$, $b_1=H+C\alpha_{pf}$, $b_2=H+C\alpha_{ps}$, $a_1=C+M\alpha_{pf}$, $a_2=C+M\alpha_{ps}$, while $k_l=\omega/c_l$ and c_l $(l=pf,ps,s)$ are the wavenumbers and velocities of the three body waves in the porous formation, i.e., the fast compressional wave, the slow compressional wave and the shear wave, $\eta_l=\sqrt{k^2-k_l^2}$ are the radial wavenumbers, α_l are the factors reflecting the amplitude ratio and phase shift between the displacements of the solid phase and the relative flow with respect to the three body waves, the expressions of c_l and α_l are given by Pride and Haartsen (1996) and Hu, Wang and Wang (2000), K_1 is the second kind modified Bessel function of first order, r_b is the borehole radius and A_{pf}, A_{ps} and A_s are the undetermined coefficients in the formulas of the acoustic fields in the porous formation. According to the Cramer rule, the solution of linear equations $\mathbf{A}x=\mathbf{b}$ composed of equations (A4)-(A7) can be written as $x_n=\Delta x_n/\Delta$ $(n=1,2,3,4)$, where Δ is the determinant of the coefficient matrix $\mathbf{A}$ and Δx_n are the determinants of the matrix obtained from $\mathbf{A}$ by replacing column n with the vector $\mathbf{b}$. The Stoneley wave pole $k=k_{st}$ makes the determinant Δ equal to zero.

Once the coefficients A_{ba}, A_{pf}, A_{ps} and A_s are determined and the acoustic fields in the borehole and formation are obtained, the undetermined coefficient A_{be} in equation (A3) can be solved from the following equations established by using the electromagnetic fields in the borehole and formation and the boundary conditions of the electromagnetic field on the borehole wall.

$$-\eta_{be}^2I_0(\eta_{be}r_b)A_{be}+\eta_{em}^2K_0(\eta_{em}r_b)A_e = \frac{T_e}{i\omega\bar{\varepsilon}}\left[ik\left(\alpha_{pf}K_0(\eta_{pf}r_b)A_{pf}+\alpha_{ps}K_0(\eta_{ps}r_b)A_{ps}\right) + \frac{k_{em}^2}{k_s^2-k_{em}^2}\alpha_s\eta_s^2K_0(\eta_sr_b)A_s\right], \tag{A8}$$

$$i\omega\bar{\varepsilon}_b\eta_{be}I_1(\eta_{be}r_b)A_{be}+i\omega\bar{\varepsilon}\eta_{em}K_1(\eta_{em}r_b)A_e = T_e\frac{k_s^2}{k_s^2-k_{em}^2}\alpha_s\eta_sK_1(\eta_sr_b)A_s. \tag{A9}$$

where k_{em} is the wavenumber of the electromagnetic wave in the formation, $\eta_{em}=(k^2-k_{em}^2)^{1/2}$ is the radial wavenumber, $T_e=-i\omega\eta L/\kappa$, $\bar{\varepsilon}=\varepsilon+i\sigma/\omega$, ε is the formation permittivity, $\bar{\varepsilon}_b=\varepsilon_b+i\sigma_b/\omega$, ε_b and σ_b are the permittivity and the conductivity of the borehole fluid, I_1 is the first kind modified Bessel function of first order and A_e is the undetermined coefficient in the formulas of the electromagnetic fields in the porous formation. It is seen that the terms acting as the source of the electromagnetic field at the right-hand side of equations (A8) and (A9) are related to the acoustic fields in the formation. Solving equations (A8) and (A9), coefficient A_{be} is obtained as

$$A_{be}(x_2,x_3,x_4)=\frac{-ikT_ex_1\psi(x_1,x_2,x_3,x_4)}{i\omega\bar{\varepsilon}_b\cdot\eta_{em}^2\eta_{be}r_b\cdot Y_{em}\cdot I_1(\eta_{be}r_b)+\eta_{be}^2\cdot i\omega\bar{\varepsilon}\cdot I_0(\eta_{be}r_b)}, \tag{A10}$$

where $Y_{em}=K_0(\eta_{em}r_b)/\eta_{em}r_bK_1(\eta_{em}r_b)$ and

$$\psi=\frac{1}{k^2x_1}\left[k^2\left(\alpha_{pf}Y_{pf}x_2+\alpha_{ps}Y_{ps}x_3\right) + \frac{k_s^2}{k_s^2-k_{em}^2}\alpha_s\left(\eta_{em}^2Y_{em}-\frac{k_{em}^2}{k_s^2}\eta_s^2Y_s\right)x_4\right]. \tag{A11}$$

Substituting the representations of the pressure and electric fields into equation (A1) and considering that the residue of the term $\omega^2\rho_b\cdot 2K_0(\eta_{ba}r_0)$ related to the point acoustic source in equation (A2) is zero, yields

$$R_{EP}(\omega)=\left.\frac{-\eta_{be}^2I_0(\eta_{be}r_0)A_{be}(\Delta x_2,\Delta x_3,\Delta x_4)}{\omega^2\rho_b\cdot\Delta x_1\cdot I_0(\eta_{ba}r_0)}\right|_{k=k_{st}}. \tag{A12}$$

Then substituting equation (A10) into equation (A12), and letting

$$R_I=\frac{k_{st}\eta_{be}I_0(\eta_{be}r_0)}{I_0(\eta_{ba}r_0)\left(i\omega\bar{\varepsilon}_b\cdot\eta_{em}^2r_b\cdot Y_{em}\cdot I_1(\eta_{be}r_b)+\eta_{be}\cdot i\omega\bar{\varepsilon}\cdot I_0(\eta_{be}r_b)\right)}, \tag{A13}$$

we have

$$R_{EP}(\omega)=\left.\frac{\eta L(\omega)}{\omega\rho_b\kappa(\omega)}R_I\psi(\Delta x_1,\Delta x_2,\Delta x_3,\Delta x_4)\right|_{k=k_{st}}. \tag{A14}$$

In the frequency range of well logging (in the order of kHz), the wavelengths of the electromagnetic wave, the fast compressional wave and the shear wave in porous formations are much larger than the borehole radius. Therefore their radial wavenumbers satisfy $r_b|\eta_{em}|\ll 1$, $r_b|\eta_{pf}|\ll 1$ and$r_b|\eta_s|\ll 1$, respectively. Note that at these frequencies the slow compressional wave in porous media is a diffusion model and thus its radial wavenumber does not satisfy asimilar inequality. Considering that the electromagnetic wavenumber is much smaller than the acoustic wavenumbers, i.e., $k_{em}^2\ll k_s^2$, $k_{em}^2\ll k_{st}^2$, we obtain$|\eta_{em}|\approx|k_{st}|$. Then using the approximation of $K_1(z)\approx 1/z$ as $z\to 0$, we have $\eta_{em}^2Y_{em}\gg(k_{em}^2/k_s^2)\eta_s^2Y_s$.

Thus equation (A11) approximates to

$$\psi|_{k=k_{st}} \approx \frac{k_{st}^2\left(\alpha_{pf}Y_{pf}\Delta x_2+\alpha_{ps}Y_{ps}\Delta x_3\right)+\alpha_s\eta_{em}^2Y_{em}\Delta x_4}{k_{st}^2\Delta x_1}. \tag{A15}$$

In order to determine the determinants Δx_n,$(n=1,2,3,4)$ in equation (A15), we firstly rewrite the three body wave velocities by the Taylor series expansion at $x=0$ as

$$c_{pf}^2=\frac{H}{\rho}\left[1+\left(\frac{\rho_f}{\rho}-\frac{C}{H}\right)^2 y\right]+o(x^2). \tag{A16}$$

$$c_{ps}^2=-i\omega C_D\left[1-\left[\left(\frac{\rho_f}{\rho}-\frac{C}{H}\right)^2+\frac{\rho_f\alpha_\infty}{\rho\phi}\left(1+\frac{2}{m}\right)-\left(\frac{\rho_f}{\rho}\right)^2\right]y+o(x^2)\right]. \tag{A17}$$

$$c_s^2=\frac{G}{\rho}\left[1+\left(\frac{\rho_f}{\rho}\right)^2 y\right]+o(x^2). \tag{A18}$$

where $x=-i\omega/\omega_c$ and $y=\rho\phi x/\rho_f\alpha_\infty$ and $C_D=\frac{\kappa_0}{\eta}\left(\frac{HM-C^2}{H}\right)$ is the diffusivity of the slow compressional wave at low frequencies. Then substituting equations (A16)-(A18) into equations (A4)-(A7) and using the representations of α_l $(l=pf,ps,s)$, we can obtain the expressions of Δx_n,$(n=1,2,3,4)$ at $k=k_{st}$. Finally substituting them into equation (A15) and then simplifying, we have

$$\psi|_{k=k_{st}}=\frac{\left(C_2\rho_b+C_1\rho_f\right)\phi x}{\alpha_\infty\rho_f}\left\{1-\left[1+\frac{2}{m}-\frac{\phi}{r_bY_{ps}\alpha_\infty\eta_{ba}}-\frac{\phi}{\alpha_\infty}\frac{C}{H}\left(1-\frac{Y_{pf}}{Y_{ps}}\right)\times\left(\frac{\eta_{em}^2Y_{em}-\eta_s^2Y_s}{k_{st}^2Y_{pf}-\eta_s^2Y_s}\right)\right]x\right\}+o(x^3). \tag{A19}$$

Because of $r_b|\eta_{ba}|\ll 1$, using the limiting forms of $I_0(q)\to 1$ and $I_1(q)\to q/2$ as $q\to 0$ (Abramowitz and Stegun 1965), we have $C_1\approx\eta_{ba}r_b/2$and $C_2\approx 1$ and thus $C_2\rho_b\gg C_1\rho_f$. By employing the parameters in Table 1, we numerically calculate the last term in the square brackets in the right-hand side of equation (A19). It is found that the following inequality is satisfied when the frequency is more than 500 Hz.

$$\frac{\phi}{\alpha_\infty}\frac{C}{H}\left(1-\frac{Y_{pf}}{Y_{ps}}\right)\left(\frac{\eta_{em}^2Y_{em}-\eta_s^2Y_s}{k_{st}^2Y_{pf}-\eta_s^2Y_s}\right)\ll 1+\frac{2}{m} \tag{A20}$$

Further calculations for various formations show that the value of the term in the left- hand side of equation (A20) has little change and the inequality is always satisfied. Thus equation (A19) is appropriately simplified as

$$\psi|_{k=k_{st}}=\frac{\phi}{\alpha_\infty}\frac{\rho_b}{\rho_f}x\left[1-\left(1+\frac{2}{m}-\frac{\phi}{r_bY_{ps}\alpha_\infty\eta_{ba}}\right)x\right]+o(x^3). \tag{A21}$$

Due to an unreasonable simplification of the term in the right-hand side of equation (A5) approximating to zero is used in Plyshchenkov and Nikitin (2010), the equation similar to equation (A21) in their works lacks the term $\phi/r_bY_{ps}\alpha_\infty\eta_{ba}$. We numerically calculate the term $\phi/r_bY_{ps}\alpha_\infty\eta_{ba}$ in equation (A21) by employing the parameters in Table 1 and find that the following inequality is satisfied when the frequency is more than 500 Hz.

$$\phi/r_bY_{ps}\alpha_\infty\eta_{ba}\ll 1. \tag{A22}$$

Further calculations for various formations indicate that: 1) equation (A22) is satisfied for high-porosity and high-permeability formations and low-porosity and low-permeability formations that have good correlations between porosity and permeability and for low-porosity and high-permeability formations whose fractures are developed and matrixes are compact; 2) equation (A22) is not always satisfied and can be even larger than 1.0 theoretically for high-porosity and low-permeability formations whose pores have too much clay. Therefore the term $\phi/r_bY_{ps}\alpha_\infty\eta_{ba}$ reflects the clay content in pores. If the effect of the clay blocking pores is not large and the inequality of equation (A22) is satisfied, equation (A21) can be simplified further as

$$\psi|_{k=k_{st}}=\frac{\phi}{\alpha_\infty}\frac{\rho_b}{\rho_f}x\left[1-\left(1+\frac{2}{m}\right)x\right]+o(x^3). \tag{A23}$$

The representations of $L(\omega)$ and $\kappa(\omega)$ can be expanded in the Taylor series at $x=0$ as

$$\frac{\eta L(\omega)}{\kappa(\omega)}=-\frac{\phi\varepsilon_f\varsigma}{\alpha_\infty\kappa_0}\left(1+\left(1-\frac{m}{8}+\frac{2}{m}\right)x+o(x^2)\right). \tag{A24}$$

Then substituting equations(A23) and (A24) into equation (A14), we finally obtain equation (4) in this paper. If we consider the pore blockage caused by the clay, the expression of the Stoneley wave REP is derived as

$$R_{EP}(\omega)=i\frac{\phi\varepsilon_f\varsigma}{\eta\alpha_\infty}\left[1+\left(\frac{\phi}{r_bY_{ps}\alpha_\infty\eta_{ba}}-\frac{m}{8}\right)\frac{-i\omega}{\omega_c}\right]R_I. \tag{A25}$$